ARL-TR-7642 ● APR 2016

US Army Research Laboratory

Generating Variable Wind Profiles and Modeling Their Effects on Small-Arms Trajectories

by Timothy A Fargus

NOTICES

Disclaimers

The findings in this report are not to be construed as an official Department of the Army position unless so designated by other authorized documents.

Citation of manufacturer's or trade names does not constitute an official endorsement or approval of the use thereof.

Destroy this report when it is no longer needed. Do not return it to the originator.

ARL-TR-7642 ● APR 2016

US Army Research Laboratory

Generating Variable Wind Profiles and Modeling Their Effects on Small-Arms Trajectories

by Timothy A Fargus
Weapons and Materials Research Directorate, ARL

REPORT DOCUMENTATION PAGE

Form Approved
OMB No. 0704-0188

1. REPORT DATE *(DD-MM-YYYY)*	2. REPORT TYPE	3. DATES COVERED (From - To)
April 2016	Final	January 2015–January 2016

4. TITLE AND SUBTITLE
Generating Variable Wind Profiles and Modeling Their Effects on Small-Arms Trajectories

5a. CONTRACT NUMBER

5b. GRANT NUMBER

5c. PROGRAM ELEMENT NUMBER

6. AUTHOR(S)
Timothy A Fargus

5d. PROJECT NUMBER

5e. TASK NUMBER

5f. WORK UNIT NUMBER

7. PERFORMING ORGANIZATION NAME(S) AND ADDRESS(ES)
US Army Research Laboratory
ATTN: RDRL-WML-A
Aberdeen Proving Ground, MD 21005-5069

8. PERFORMING ORGANIZATION REPORT NUMBER
ARL-TR-7642

9. SPONSORING/MONITORING AGENCY NAME(S) AND ADDRESS(ES)

10. SPONSOR/MONITOR'S ACRONYM(S)

11. SPONSOR/MONITOR'S REPORT NUMBER(S)

12. DISTRIBUTION/AVAILABILITY STATEMENT
Approved for public release; distribution is unlimited.

13. SUPPLEMENTARY NOTES

14. ABSTRACT
It is a common practice in modeling the trajectories of direct-fire munitions to assume that the crosswind is constant across the whole range of the projectile's flight. We know, however, that this is not how wind behaves. Through application of wind variation methodologies and data analysis on the variation of wind versus range, we developed a metric, called Equivalent Constant Crosswind, which allows for the effects of variable crosswind to be modeled without having to explicitly model the variation of the wind at every step.

15. SUBJECT TERMS
small arms, direct fire, wind, variable wind, projectile flight

16. SECURITY CLASSIFICATION OF:			17. LIMITATION OF ABSTRACT	18. NUMBER OF PAGES	19a. NAME OF RESPONSIBLE PERSON
a. REPORT	b. ABSTRACT	c. THIS PAGE			Timothy A Fargus
Unclassified	Unclassified	Unclassified	UU	42	19b. TELEPHONE NUMBER (Include area code) 410-278-6111

Contents

List of Figures

List of Tables

1. Introduction

Currently, a common practice in wind modeling for small-arms applications is to assume that a constant crosswind exists across the entire range to a target. We know, however, that wind does not behave this way in reality. Analysis and study of the behavior of wind can help efforts to understand and reduce the delivery error attributed to crosswind.

The first goal of this study was to develop a methodology to generate synthetic wind fields (i.e., the crosswind as a function of location at a fixed point in time) based on empirical data. The ability to incorporate synthetic wind fields into existing simulations will increase those models' accuracy and provide us with a better understanding of weapon accuracy. The differences between the effects of constant crosswind across all ranges and the effects of variable wind are likely small at close ranges, but in long-range applications the difference can be large, and we could be underestimating or overestimating the magnitude of deflection due to crosswind at range.

This could, in turn, lead to an overestimation or underestimation of the gains in accuracy from a wind estimation and correction system. Moreover, the ability to model variable wind will give us the ability to more accurately model the performance of these systems directly. With an explicitly modeled synthetic wind field we can better model the performance of a system that estimates and corrects for that wind.

The second goal of this study was to develop a metric called Equivalent Constant Crosswind (ECC), which allows for the effects of variable crosswind on a downrange projectile to be modeled without having to explicitly model the variation of the wind at every step. This will allow for easy incorporation of wind fields into existing models without extensive changes and without substantially increasing the runtimes required.

To accomplish the study goals, we analyzed a set of crosswind data obtained from an anemometer array at Fort Benning in December 2012 and investigated several methodologies to simulate the observed variation of crosswind with range, including treating each anemometer independently, autoregressive models of order p (where the previous p crosswind measurements are used to determine the next crosswind value), and sampling against a multivariate normal distribution.

We ran a Monte Carlo analysis over a matrix of input parameters to determine the effect of those parameters on ECC. The parameters most relevant to this analysis were shooter-to-target range, muzzle velocity, projectile mass, drag coefficient

exponent, wind standard deviation (i.e., the standard deviation of the crosswind magnitude at the measurement points over time), and spatial wind correlation.

Section 2 will summarize the analysis done on the data set obtained at Fort Benning in 2012. Section 3 will detail the methodology for using McCoy's lag time methodology alongside the Weinacht-Cooper-Newill (WCN) projectile flyout methodology to obtain measures of ECC. Section 4 will briefly summarize the ECC results obtained from the observed data and the assumptions made in obtaining them. Section 5 will outline the different approaches used to model the observed wind behavior. Section 6 will present the recommendations for how to use the model that fits the data best along with the effects of changing different variables. Section 7 will present the conclusion.

2. Analyzing Wind Data

In December 2012, a set of wind values was collected at Fort Benning. Ten anemometers (A_1–A_{10}) were placed along a straight line spaced 110 m apart. Wind speed and direction were recorded every second for just over 3 h, and from these values the crosswind and range wind were derived. For our purposes, crosswind is defined as the component of the wind perpendicular to the line connecting the anemometers, with positive crosswind values to the right as you look from A_1 to A_{10}, and range wind is defined as the component of the wind parallel to the line connecting the anemometers, with positive range wind in the direction of ascending anemometer numbers. Because crosswind is a much bigger contributor to deflection at range than range wind, we only analyzed the crosswind component of the data set.

The crosswind measurements from each anemometer were analyzed for normality and were found in most cases to be close to normal.[1] A couple of the locations showed a somewhat pronounced skew. Figure 1 is a histogram of the measured crosswind velocities at A_3 that appear to be roughly normal. Figure 2 is a histogram of the measured crosswind velocities at A_4 that show a pronounced skew. To simplify calculations when modeling variable wind fields, the wind measurements at each station were assumed to be normal.[2]

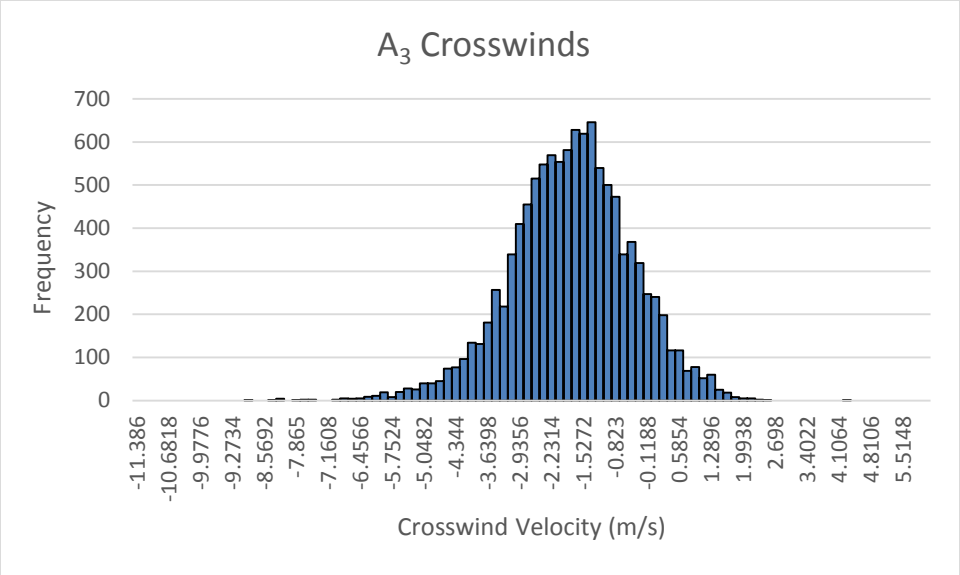

Fig. 1 Histogram of measured crosswind values from A_3

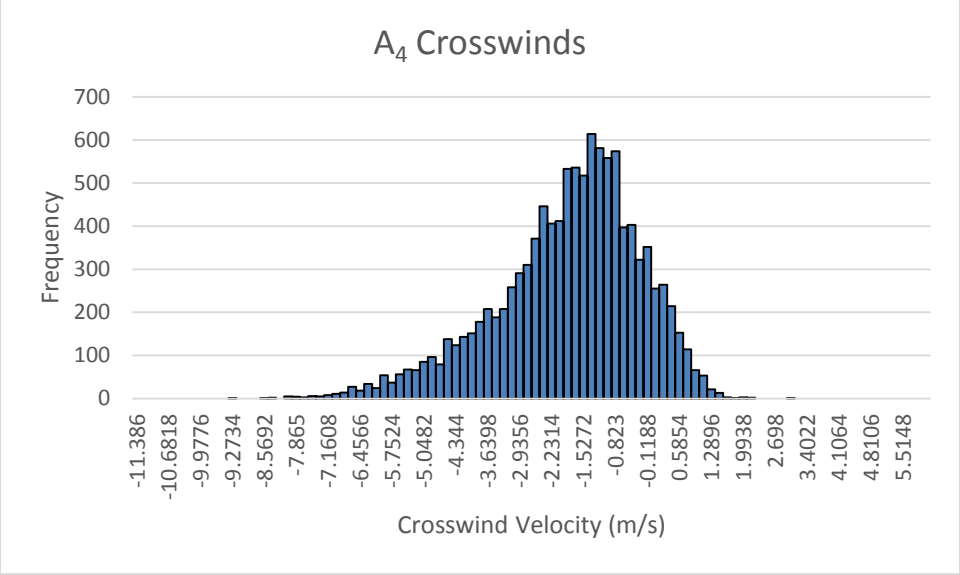

Fig. 2 Histogram of measured crosswind values from A_4

Mean and standard deviations of the crosswind velocities at each anemometer were also obtained from the data and are shown in Table 1 and graphically in Figs. 3 and 4. For these calculations, each measurement (taken at the same location approximately once per second) was assumed to be an independent sample.

Table 1 Crosswind means and standard deviations (in meters/second)

	A_1	A_2	A_3	A_4	A_5	A_6	A_7	A_8	A_9	A_{10}
Mean	–1.55	–1.59	–1.71	–1.77	–1.47	–2.69	–1.41	–2.74	–2.93	–3.01
Std. Dev.	1.28	1.55	1.34	1.59	1.58	1.99	1.61	1.83	1.59	1.72

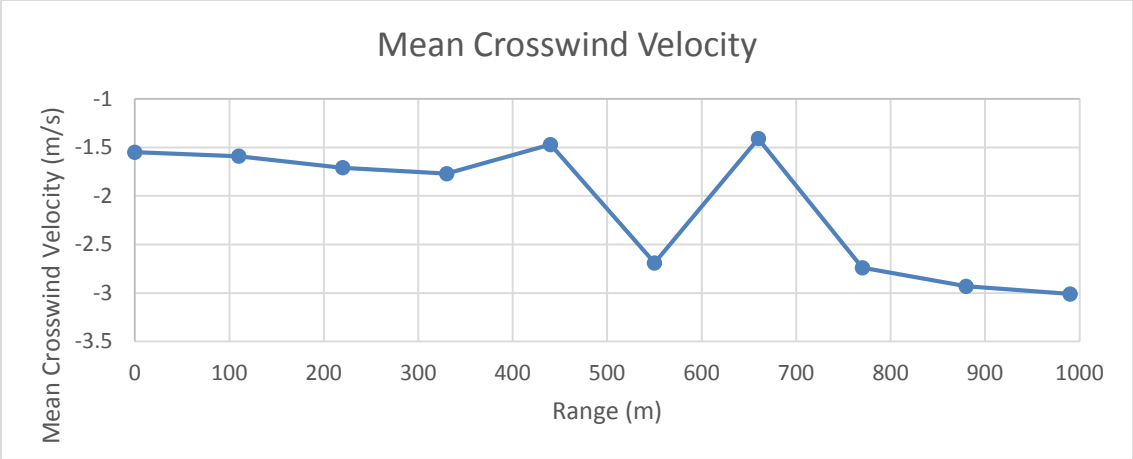

Fig. 3 Mean crosswind velocity vs. range

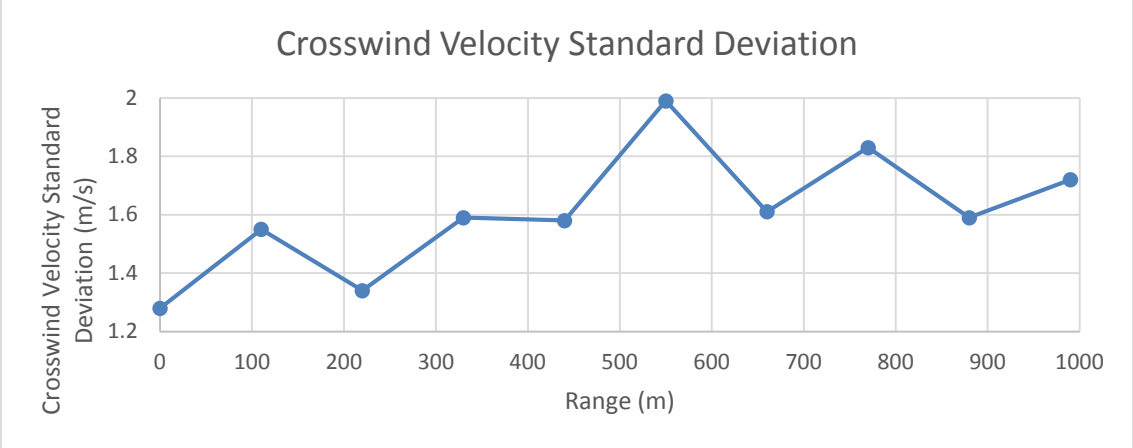

Fig. 4 Crosswind standard deviation vs. range

For the remainder of the report, the mean and standard deviation of the crosswind at anemometer A_n will be denoted μ_n and σ_n, respectively. Instances of the crosswind at anemometer A_n will be denoted W_n.

To model the behavior of the crosswind accurately we first had to determine the correlation between the observed wind values. We can easily determine the correlation coefficient ρ between stations A_n and A_m by the following equation (Box 1976):

$$\rho(A_n, A_m) = \frac{cov(W_n, W_m)}{\sigma_n \sigma_m}. \quad (1)$$

This generated Table 2, which lists correlation coefficients between each pair of stations. A correlation coefficient of 1.0 indicates total positive correlation between 2 variables, meaning that a linear equation describes their relationship perfectly. A correlation coefficient of 0 indicates no linear correlation between 2 variables. Values in between indicate varying levels of positive correlation between variables.

Table 2 Pairwise correlation coefficients between anemometers

	A_1	**A_2**	**A_3**	**A_4**	**A_5**	**A_6**	**A_7**	**A_8**	**A_9**	**A_{10}**
A_1	1.00	0.27	0.16	0.21	0.20	0.25	0.21	0.17	0.17	0.18
A_2	0.27	1.00	0.19	0.20	0.29	0.23	0.22	0.19	0.18	0.17
A_3	0.16	0.19	1.00	0.23	0.27	0.30	0.24	0.21	0.21	0.21
A_4	0.21	0.20	0.23	1.00	0.32	0.32	0.31	0.28	0.25	0.25
A_5	0.20	0.29	0.27	0.32	1.00	0.36	0.34	0.30	0.29	0.24
A_6	0.25	0.23	0.30	0.32	0.36	1.00	0.53	0.43	0.39	0.35
A_7	0.21	0.22	0.24	0.31	0.34	0.53	1.00	0.48	0.36	0.34
A_8	0.17	0.19	0.21	0.28	0.30	0.43	0.48	1.00	0.43	0.41
A_9	0.17	0.18	0.21	0.25	0.29	0.39	0.36	0.43	1.00	0.47
A_{10}	0.18	0.17	0.21	0.25	0.24	0.35	0.34	0.41	0.47	1.00

For the remainder of this report, correlation coefficients between stations A_n and A_m will be denoted $\rho_{n,m}$. There is no difference between $\rho_{n,m}$ and $\rho_{m,n}$, but the preference will be for the smaller number to be listed in the subscript first.

In the next section, we will explain in some depth the methodology used to analyze the observed crosswind data and ultimately to generate synthetic wind fields.

3. Calculation of Horizontal Deflection and Equivalent Constant Crosswind

To determine the horizontal deflection imparted by a variable crosswind on a projectile at its target, we used a combination of equations detailing deflection due to variable crosswind (McCoy 1976) and the WCN equations detailing trajectories of direct-fire munitions (Weinacht et al. 2005).

3.1 McCoy Methodology for Deflection at Range Due to Crosswind

To determine the horizontal deflection (Z_{R_i}) imparted at range R by a constant crosswind occurring between ranges X_{i-1} and X_i (for $X_i, X_{i+1} \leq R$), McCoy (1976) gives the following equation[3]:

$$Z_{R_i} = W_{Z_{(i-1,i)}} \left\{ \left[t_R - t_{X_{i-1}} - \frac{R - X_{i-1}}{V_{X_{i-1}}} \right] - \left[t_R - t_{X_i} - \frac{R - X_i}{V_{X_i}} \right] \right\}, \quad (2)$$

where

$W_{Z_{(i-1,i)}}$ = magnitude of crosswind between ranges X_{i-1} and X_i,

t_{X_i} = time of flight of the projectile to range X_i, and

V_{X_i} = residual velocity of the projectile at range X_i.

The term $t_R - t_{X_i} - \frac{R - X_i}{V_{X_i}}$ in Eq. 2 represents the difference between actual flight time between range X_i and range R and the time between the same ranges in a vacuum. This is commonly referred to as "lag time".

If there is a set of monotonically increasing ranges $\{X_0, X_1, X_2, \ldots, X_n\}$, $X_i \leq R \; \forall \; i \leq n$, and a corresponding set of crosswinds $\left\{W_{Z_{(0,1)}}, W_{Z_{(1,2)}}, \ldots, W_{Z_{(n-1,n)}}\right\}$ where crosswind between ranges X_{i-1} and X_i is constant and equal to $W_{Z_{(i-1,i)}}$, then the total horizontal deflection at range R due to crosswind is equal to

$$Z_R = \sum_{i=1}^{n} Z_{R_i} \, . \quad (3)$$

It stands to reason that there exists a constant crosswind that would have produced the same horizontal deflection as any particular variable wind field. If we apply Eq. 2 across a trajectory with constant crosswind W_Z, range R, and time of flight t, we arrive at the following equation for Z_R:

$$Z_R = W_Z \left[t - \frac{R}{V_0} \right]. \quad (4)$$

By combining Eqs. 3 and 4 and solving for W_Z, the constant crosswind that would produce the same deflection, or ECC, is given by

$$ECC = W_Z = \frac{\sum_{i=1}^{n} Z_{R_i}}{t - \frac{R}{V_0}} \, . \quad (5)$$

3.2 Incorporation with WCN Model

The calculation of ECC depends on time of flight and residual velocity for every range X_i used as an input. To determine these quantities at a given range for a general case that correctly models flight in the transonic and subsonic regimes, we use the WCN methodology (Weinacht 2014). A closed-form solution can be used if the projectile's velocity remains supersonic. This solution is outlined in

Appendix A. For cases where flight crosses velocity regimes, we use Oberle's implementation of the WCN methodology (Oberle 2009).

Under the assumption that the drag curve is continuous, Oberle's model requires the following inputs:

- Muzzle velocity
- Drag coefficient at the muzzle velocity
- Drag coefficient exponent in the supersonic velocity regime
- Transition Mach number between transonic and supersonic velocity regimes
- Transition Mach number between subsonic and transonic velocity regimes
- Drag coefficient in the subsonic velocity regime ($C_D|_{Sub}$)
- Muzzle retardation

If we are to investigate notional projectiles with modified mass and velocity, we must have expressions that allow us to find the corresponding muzzle retardation and drag coefficient at the muzzle velocity. Muzzle retardation is expressed as follows:

$$\left(\frac{dV}{ds}\right)_0 = \frac{-1}{2m}\rho V_0 S_{ref} C_D|_{V_0}\,, \tag{6}$$

where

m = projectile mass,

ρ = air density,

S_{ref} = reference area of the projectile, and

$C_D|_{V_0}$ = drag coefficient at muzzle velocity.

If we know the air density as well as the mass, muzzle retardation, and reference area of the projectile, we can solve Eq. 6 for $C_D|_{V_0}$ as a function of known quantities and not specify it explicitly.

$$C_D|_{V_0} = \frac{-2m\left(\frac{dV}{ds}\right)_0}{\rho V_0 S_{ref}}\,. \tag{7}$$

Oberle includes the following expression for deriving muzzle retardation from a known set of values for bullets with the same basic shape and reference area but with different mass and muzzle velocity values.

$$\left(\frac{dV}{ds}\right)_{New} = \left(\frac{dV}{ds}\right)_{Known} \left(\frac{m_{Known}}{m_{New}}\right) \left(\frac{V_{New}}{V_{Known}}\right)^{1-n} . \quad (8)$$

Quantities with the *Known* subscript refer to known values and quantities with the *New* subscript refer to modified velocity and mass. This means that if there is an array of associated muzzle velocity, muzzle retardation, and mass and drag coefficient exponent values, then muzzle retardation can be expressed as a function of those values and modified mass and/or muzzle velocity values.

Thus muzzle retardation and drag coefficient at the muzzle can be removed as independent variables in favor of mass, air density, and reference area, and the list of required inputs is modified to the following:

- Muzzle velocity
- Projectile mass
- Projectile reference area/diameter
- Air density
- Set of associated supersonic drag coefficient exponents, muzzle velocities, muzzle retardations, and masses
- Transition Mach number between transonic and supersonic velocity regimes (assumed to be 1.05 for this analysis)
- Transition Mach number between subsonic and transonic velocity regimes (assumed to be 0.85 for this analysis)
- Drag coefficient in the subsonic velocity regime

Using these inputs, the trajectories can then be run using Oberle's implementation of the WCN model.

4. Analysis of Equivalent Constant Crosswind from Wind Data

We first analyzed the behavior of the ECC of the Fort Benning wind data. The results of this analysis became the standard against which we judged the performance of our proposed synthetic wind field models. The data set included crosswind values at each of the 10 anemometers at 11,085 different fixed times. We treated these as independent samples for the purpose of this analysis. We assumed that the crosswind values measured at each station at the time the shot was fired would be the crosswind values experienced by the projectile when it arrived at that station. That is, time variation of the crosswind during a trajectory did not enter into the calculation of deflection. Second, we assumed that the crosswind at any

trajectory location was equal to the measured crosswind value at the closest anemometer.

Adjacent anemometers were separated by 110 m in a straight line from 0 to 990 m. We determined that our ranges of interest were every 55 m from the shooter to the target; that is, at each anemometer and at each point equidistant from 2 adjacent anemometers. This split the range into 18 subsections with each assumed to have constant wind within them. To find the ECC for a given range R, we used Eq. 2 to determine the deflection induced at R by the wind on each interval and then we summed those deflections and input the sum into Eq. 5 to obtain the ECC.

We used the WCN methodology to find the time of flight and residual velocity at each range of interest using the M855/M4 weapon/ammunition combination $V_0 = 866\,m/s,\ m = 4\,g,\ d = 5.56mm,\ \left(\frac{dV}{ds}\right)_0 = -1.028,\ n = 0.53,\ C_D|_{Sub} = 0.198,\ \rho = 1.225\,kg/m\text{^}3$. ECC depends on the variables that describe the behavior of the wind (mean and standard deviation at each location and correlation between locations) as well as the inputs that describe the flight of the particular projectile being analyzed. Section 6 and Appendix B go into greater detail about how much the ECC's behavior depends on each of these inputs. Figure 5 shows the mean ECC value versus range from the Fort Benning data set (μ_{ECC_B}), and Fig. 6 shows the standard deviation of ECC versus range (σ_{ECC_B}).

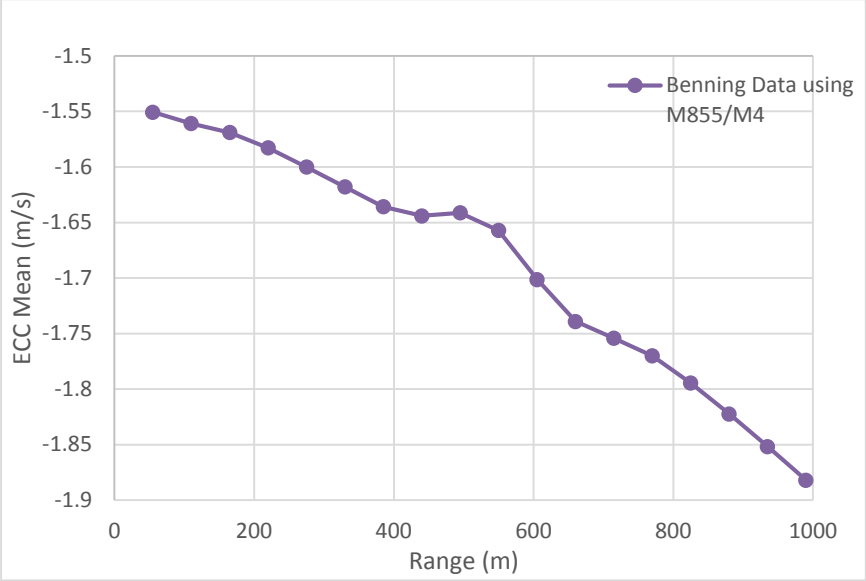

Fig. 5 Mean values of μ_{ECC_B} vs. range observed at Fort Benning

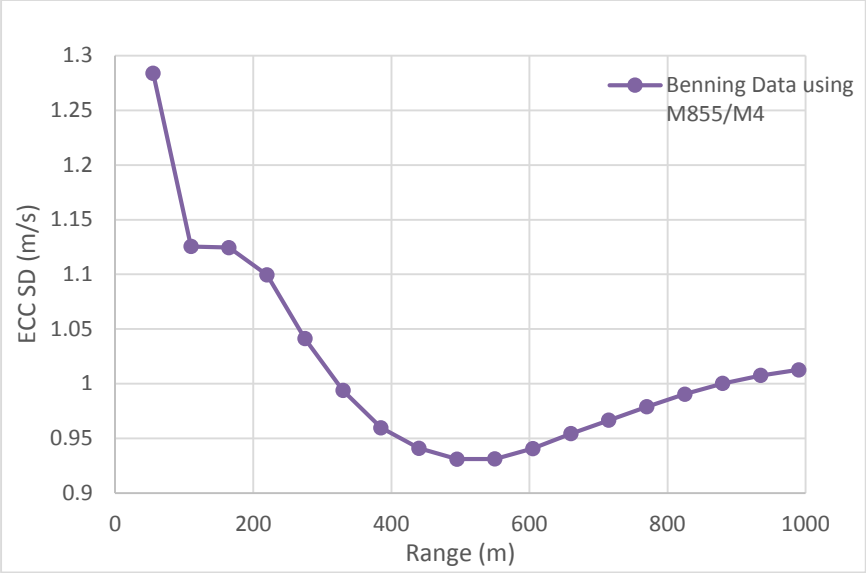

Fig. 6 Standard deviation values of σ_{ECC_B} vs. range observed at Fort Benning

The value of μ_{ECC_B} decreases with range because the means of the winds get stronger in the negative direction as range increases, as shown in Table 1. The value of σ_{ECC_B} decreases with range until halfway downrange, at which point it begins to increase gently. The increase in the longer ranges appears to be a consequence of standard deviation of measured crosswind increasing with range, shown in Table 1, and the increase in correlation among anemometers A_6–A_{10}, shown in Table 2 (the correlation values among anemometers A_1–A_5 range from 0.16 to 0.32; the correlation values among anemometers A_6–A_{10} range from 0.34 to 0.53).

The distributions of ECC at each range were found to behave similarly to the distributions of the crosswind measurements at each range.[4] Figure 7 shows the distribution of ECC values at 110 m, which appears to be approximately normal. Figure 8 shows the distribution of ECC values at 990 m, which has some irregularity including a small secondary local maximum to the left of the mean.

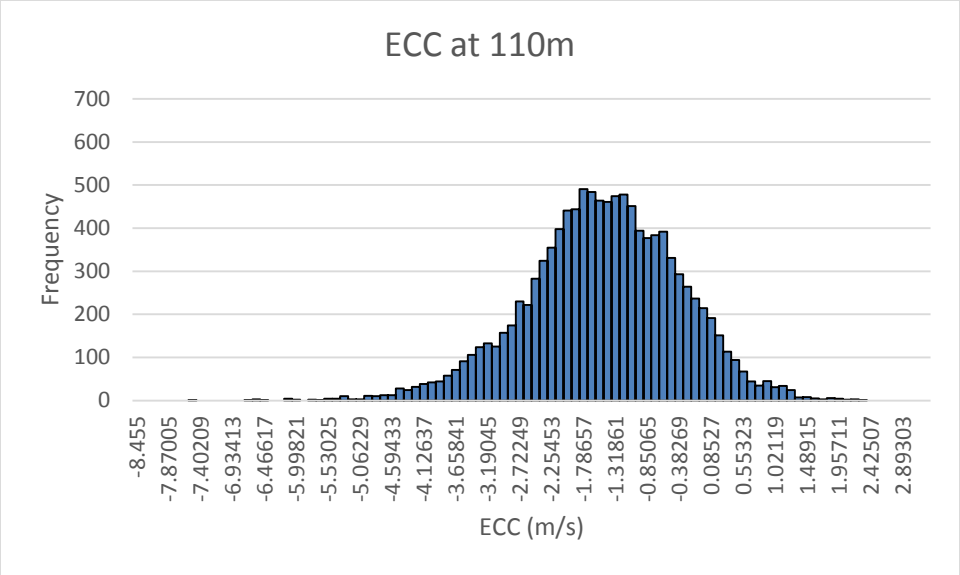

Fig. 7 Histogram of calculated ECC values at 110 m

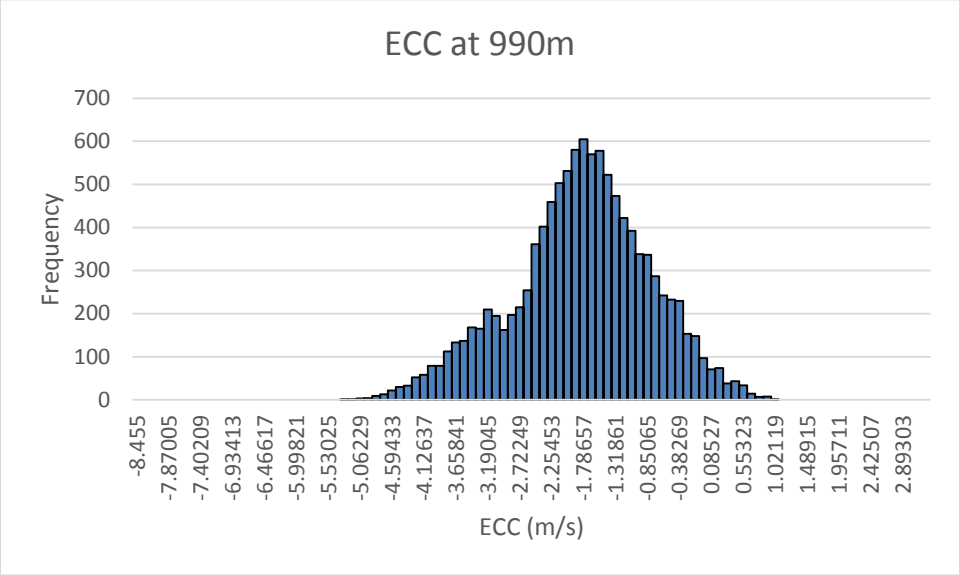

Fig. 8 Histogram of calculated ECC values at 990 m

5. Generating Synthetic Wind Fields

Next we attempted to find a model that could reproduce the behavior of the wind in the Fort Benning data set as closely as possible. We first generated a wind field by drawing the wind at each station independently using μ_n and σ_n at each station A_n. This produced σ_{ECC} results that diverged unacceptably from σ_{ECC_B}. Next we implemented an autoregressive model, which generated each wind measurement from some number of the measurements that preceded it. This model generated

σ_{ECC} results much closer to σ_{ECC_B}, but the fact that it depended on assigning an arbitrary directionality to the wind measurement locations introduced an ambiguity to its implementation that led us to investigate alternate methodologies. Further discussion of the foregoing methodologies is included in Appendix C. To refine the results from the independent and autoregressive models, it is necessary to find a model that not only preserves the distributions of measured wind at each station, but the correlations between all pairs of stations.

Upon investigation, a multivariate normal distribution addresses all of these concerns. If we let 1) $\vec{W}$ be an n-dimensional vector whose components are random variables $W_1, W_2, \ldots, W_n$, 2) Σ, the covariance matrix, be an n × n matrix whose i,jth entry is the covariance of W_i and W_j, 3) $\vec{Z}$ be an n-dimensional vector whose components are independent standard normal variates, and 4) $\vec{\mu}$ be an n-dimensional vector whose ith entry is $E(W_i)$, then

$$\vec{W} = \vec{\mu} + A\vec{Z}\,, \tag{9}$$

where A is an n × n matrix such that $A\,A^T = \Sigma$ (Gentle 2009).

This is a comparatively easy model to implement. The most complicated part is the calculation of the matrix A. One type of matrix with this property is known as the Cholesky decomposition, and there is a straightforward process by which it can be calculated (Golub 1996).

The number of iterations to run in each Monte Carlo simulation was determined by the following formula (Oberle 2015):

$$n = \left(\frac{z\alpha/_2\,\sigma}{\Delta}\right)^2, \tag{10}$$

where

n = number of iterations,

$z\alpha/_2$ = standard normal z-score corresponding to a confidence interval of 100(1- α)%,

σ = predicted standard deviation of the data, and

Δ = half length of the confidence interval.

We calculated the number of iterations using the chosen value of wind standard deviation as σ, a confidence level 100(1- α)% of 98%, and an interval half-length Δ of 0.01 m/s. We used a wind standard deviation of 1.30 m/s to yield 91,461 iterations, which we rounded up to 100,000.

With 100,000 runs, it is easy to verify that μ_n and σ_n is preserved for all n and that all of the pairwise correlations between stations are preserved. Figure 9 shows the results of a comparison of $\sigma_{ECC_{MVN}}$ with σ_{ECC_B}.

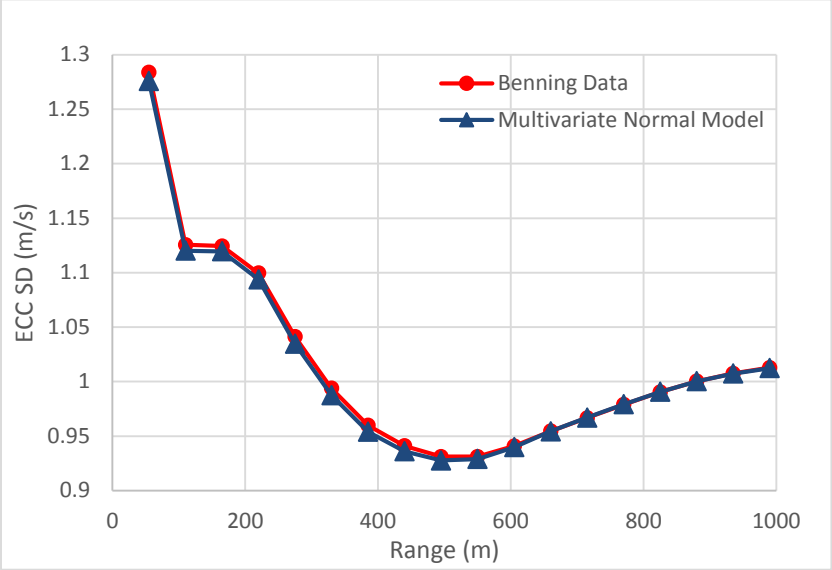

Fig. 9 Multivariate normal sampling σ_{ECC} results

Using this method, $\sigma_{ECC_{MVN}}$ differed from σ_{ECC_B} by no more than 1% at any range. As with the other models, $\mu_{ECC_{MVN}}$ remains within 1% of μ_{ECC_B} at all ranges.

6. Effects of Wind Field Changes

The aim of this report is to develop a model that can be used to generate general crosswind fields based on a set of inputs. We can make small changes to the observed data to see how changes to various inputs affect the ECC output.

Changing the wind standard deviation roughly represents a vertical stretch or compression of the σ_{ECC} versus range curve, as shown in Fig. 10. Uniformly halving σ_n for all n has the effect of halving σ_{ECC} at each range. Adding 50% to σ_n for all n has the effect of adding 50% to σ_{ECC} at each range.

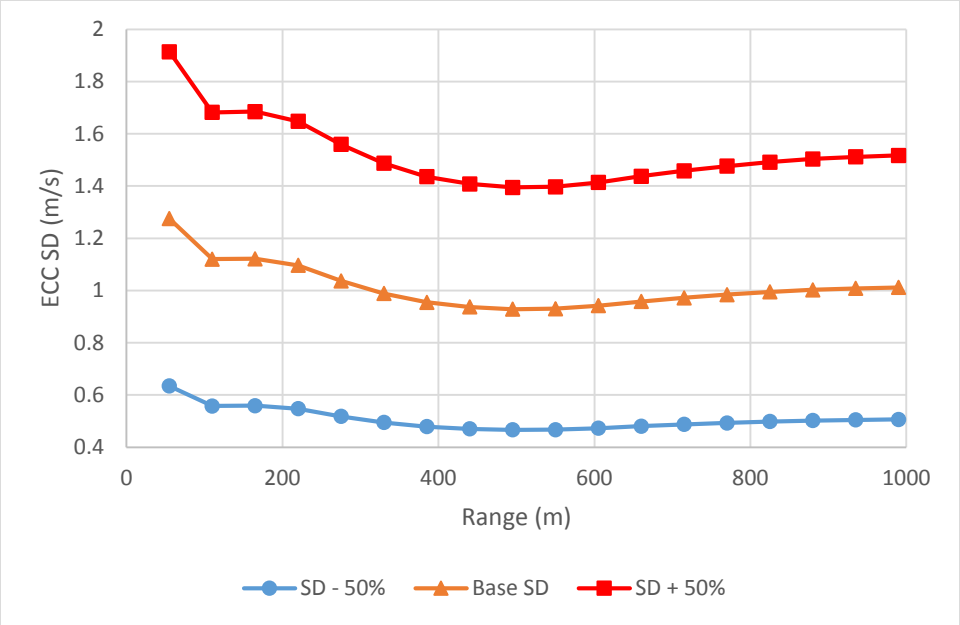

Fig. 10 Comparison of σ_{ECC} at different values of wind standard deviation

Changing the correlation values changes the slope of the σ_{ECC} versus range curve. In Fig. 11 we tested 3 levels of correlation. The baseline case was the one outlined in Table 2. In the low correlation case we subtracted 0.1 from each observed correlation. In the high correlation case we added 0.1 to each observed correlation (apart from the self-correlations, which were left at 1.0). The higher the correlation, the closer σ_{ECC} stays to the initial chosen value of the wind standard deviation.

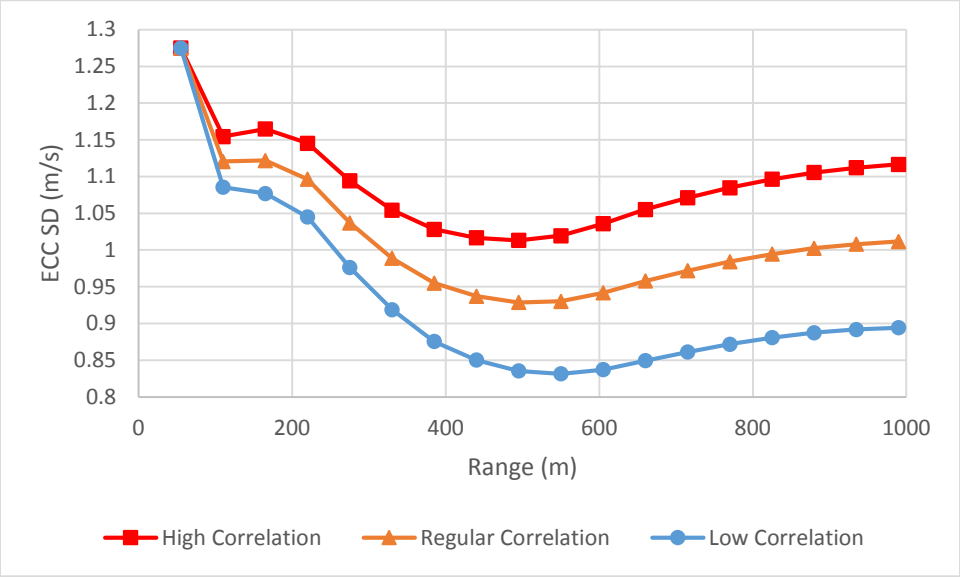

Fig. 11 Comparison of σ_{ECC} at different levels of correlation

In the data set obtained from Fort Benning, $\sigma_1 < \sigma_n$ for all $n \neq 1$, yet $\sigma_{ECC} < \sigma_1$ for all $n > 1$, despite a small increase starting around 500 m. This is because the winds at individual anemometers are only weakly correlated, meaning there is a strong possibility that winds at separate stations act in opposing directions and partially cancel each other out. As shown in Fig. 11, with higher correlations among anemometers, σ_{ECC} falls less with range than it does with lower correlations since more highly correlated winds are more likely to act in the same direction.

The small increase in σ_{ECC} observed from 500 to 1,000 m with this particular data set is caused by 2 factors: 1) σ_n tends to increase with range and 2) $\rho_{n,m}$ is uniformly greater when $6 \leq n, m \leq 10$ than when $1 \leq n, m \leq 5$. Figure 11 shows that an increase in correlation causes an increase in σ_{ECC}. In this case, when a projectile flies through the ranges covered by anemometers A_6–A_{10}, it is more likely to encounter crosswinds acting in concert with each other and therefore compounding the deflection at the target rather than canceling each other out.

We found that σ_{ECC} depended on σ_n and $\rho_{n,m}$ but not μ_n. Conversely, μ_{ECC} depended only on μ_n and not on σ_n or $\rho_{n,m}$. Figure 12 shows μ_{ECC} for the 3 correlation scenarios previously described, and the curves overlap completely. The result is the same for any cases that use the same μ_n for all n.

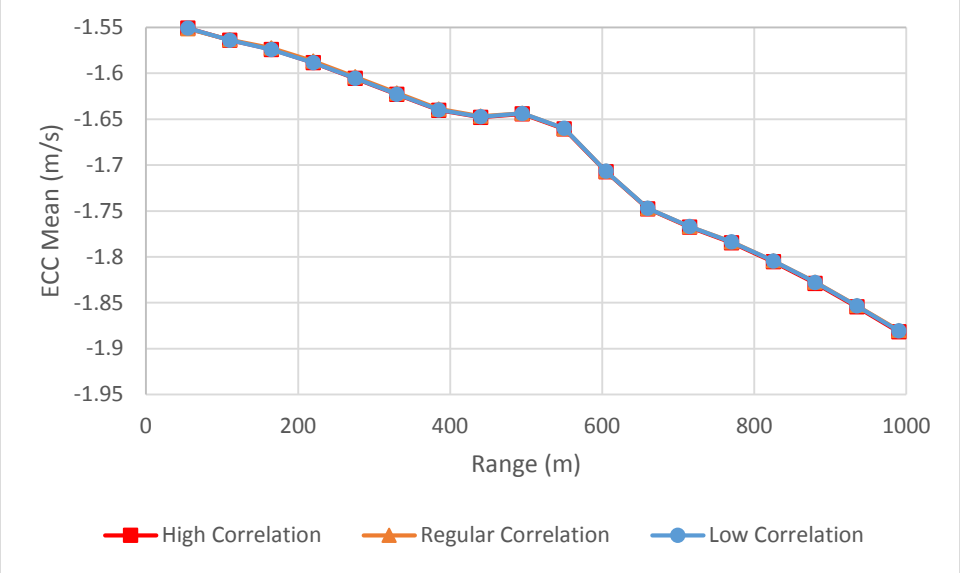

Fig. 12 Comparison of μ_{ECC} at different levels of correlation

Changes in ballistic inputs had very little impact on the value of σ_{ECC}. However, this does not mean the deflection produced by crosswind is almost identical for all rounds irrespective of drag, muzzle velocity, and mass. Rounds with higher muzzle velocities as well as heavier rounds experience less deflection due to crosswind because their time of flight to the target is lower. The drag exponent has a second-

order effect on the round's velocity over its flight and thus plays a much smaller role than mass and velocity in determining the deflection of the round due to crosswind. Graphs presenting these results are included in Appendix C. The fact that the ballistic inputs had little impact on the σ_{ECC} values indicates that we can get a good approximation of σ_{ECC} for many classes of projectiles by explicitly modeling it for only one configuration.

7. Conclusion

This report has presented a way to generate synthetic wind fields over ranges relevant to small-arms fire and argues that variable wind fields appear to behave according to a multivariate normal distribution. First we tried modeling wind measurements independently, but the modeled wind behavior did not align well enough with the observed data. An autoregressive model brought us closer to matching the observed results but exhibited ambiguity about exactly how to configure the model. In addition, the autoregressive model used only wind measurements from one direction to generate new wind measurements, but ideally the model should be independent of the direction the shooter is facing. Sampling against a multivariate normal distribution was found to strongly correlate to the observed wind across all metrics and operates independently of the locations of the shooter and target.

We developed a metric to measure the effect induced by a variable crosswind experienced by a projectile throughout its trajectory. For any deflection induced by crosswind at the target range there has to be a constant crosswind that, if applied over the whole range, would have produced that same deflection. This was designated the ECC, and analysis was performed to characterize its behavior with respect to a number of different inputs to the model.

We found that the ECC at a given range behaved according to a normal distribution, and that σ_{ECC} tends to fall as range increases for cases where the wind standard deviation and correlation are constant across the whole range. In the case of the data from Fort Benning, the wind standard deviation varied at each station, which along with a variation in correlation led to a small increase in σ_{ECC} at longer ranges. Even in the case of the data from Fort Benning, though the value of σ_{ECC} increases, the maximum value it attains is at least 20% less than the minimum wind standard deviation measured at any single location. This implies that using a constant standard deviation derived from any one measurement location to model crosswind across the whole range will tend to overestimate the horizontal error due to crosswind, though the overestimation is comparatively small at shorter ranges. The factors with the greatest impact on σ_{ECC} were the range of projectile travel, the standard deviation of crosswind measurement, and correlation between crosswind

measurements. Ballistic characteristics of the projectile such as mass, drag coefficient exponent, and muzzle velocity had comparatively little impact on the behavior of ECC.

The mechanism driving the decline in σ_{ECC} with range appears to be decreasing correlation of crosswind measurements with increasing spatial separation. Any 2 winds separated by only a short distance tend to be more strongly correlated, but as range between crosswind measurements increases, that correlation fades. The crosswind values at distant ranges become only weakly correlated with the crosswind value at the shooter's location, which makes downrange winds more likely to push in opposing directions the farther the projectile flies.

The ability to model synthetic wind fields will better allow analysis of the effectiveness of wind correction methodologies where wind is read at multiple points downrange compared with the effectiveness of correcting using the wind at the shooter's location in the presence of variable wind. Further experiments could provide better data for long-term wind standard deviation and spatial wind variability at various locations, times of day, and times of year.

8. Notes

1. Anderson-Darling and Kolmogorov-Smirnov tests indicated a departure from normality but show very high sensitivity for sample sizes as large as those used here; skewness test indicated approximate symmetry with a persistent small-to-moderate negative skew at all ranges, and kurtosis test indicated all ranges were slightly leptokurtic.
2. Time variation of wind was not taken into account for this analysis; further study of variation of wind in both space and time may refine understanding of the underlying distribution of the wind.
3. Notation has been adjusted from what appears in the source.
4. As before, Anderson-Darling and Kolmogorov-Smirnov indicated departures from normality; skewness indicated approximate symmetry with a small but persistent negative skew across all ranges and kurtosis indicated that all but the 2 furthest ranges were somewhat leptokurtic.

9. References

Box GEP, Jenkins GM. Time series analysis: forecasting and control. San Francisco (CA): Holden-Day; 1976. p. 51–52.

Deserno M. How to generate exponentially correlated Gaussian random numbers. Los Angeles (CA): UCLA Department of Chemistry and Biochemistry; 2002 Aug [accessed 2016 Jan 28]. http://www.cmu.edu/biolphys/deserno/pdf/corr_gaussian_random.pdf.

Gentle J. Computational statistics. New York (NY): Springer; 2009. p. 315–316.

Golub G, Van Loan C. Matrix computations. Baltimore (MD): The Johns Hopkins University Press; 1996. p. 145.

McCoy RL. The effect of wind on flat-fire trajectories. Aberdeen Proving Ground (MD): Army Ballistic Research Laboratory (US); 1976 Aug. Report No.: 1900.

Oberle W. Implementation of the analytical prediction of trajectories for high-velocity direct-fire munitions developed by Weinacht P, Cooper GR, and Newill JF. Aberdeen Proving Ground (MD): Army Research Laboratory (US); 2009 Feb. Report No.: ARL-MR-0714.

Oberle W. Monte Carlo simulations: number of iterations and accuracy. Aberdeen Proving Ground (MD): Army Research Laboratory (US); 2015 Jul. Report No.: ARL-TN-0684.

Valley S. Handbook of geophysics and space environments. Bedford (MA): Air Force Cambridge Research Laboratories; 1965 Apr.

Weinacht P, Cooper GR, Newill JF. Analytical prediction of trajectories for high-velocity direct-fire munitions. Aberdeen Proving Ground (MD): Army Research Laboratory (US); 2005 Aug. Report No.: ARL-TR-3567.

Weinacht PA. Direct-fire trajectory model for supersonic, transonic, and subsonic projectile flight. Aberdeen Proving Ground (MD): Army Research Laboratory (US); 2014 July. Report No.: ARL-TR-6998.

INTENTIONALLY LEFT BLANK.

Appendix A. Synthesis of McCoy and Weinacht-Cooper-Newill Methodologies

Weinacht[1] gives the following expressions to determine the time of flight and residual velocity of a projectile in the supersonic range:

$$V_{X_i} = V_0 \left\{1 + n\left(\frac{dV}{ds}\right)_0 \frac{X_i}{V_0}\right\}^{\frac{1}{n}} \quad , n \neq 0 \, . \tag{A-1}$$

$$V_{X_i} = V_0 e^{\left(\frac{dV}{ds}\right)_0 \frac{X_i}{V_0}} \quad , n = 0 \, . \tag{A-2}$$

$$t_{X_i} = \frac{1}{(n-1)\left(\frac{dV}{ds}\right)_0}\left[\left\{1 + n\left(\frac{dV}{ds}\right)_0 \frac{X_i}{V_0}\right\}^{1-\frac{1}{n}} - 1\right], n \neq 0, n \neq 1 \, . \tag{A-3}$$

$$t_{X_i} = \frac{1}{\left(\frac{dV}{ds}\right)_0} \ln\left\{1 + \left(\frac{dV}{ds}\right)_0 \frac{X_i}{V_0}\right\} \quad , n = 1 \, . \tag{A-4}$$

$$t_{X_i} = \frac{1}{\left(\frac{dV}{ds}\right)_0}\left[1 - e^{-\left(\frac{dV}{ds}\right)_0 \frac{X_i}{V_0}}\right] \quad , = 0 \, , \tag{A-5}$$

where

V_0 = muzzle velocity,

$\left(\frac{dV}{ds}\right)_0$ = muzzle retardation (s^{-1}), and

n = exponent defining the shape of the drag versus Mach number curve (unitless).

These equations can be combined with Eq. 2, given by McCoy,[2] to produce closed-form expressions for the horizontal deflection imparted at range R on a projectile that remains supersonic throughout its flight by a constant crosswind between ranges X_{i-1} and X_i in terms of crosswind velocity between X_{i-1} and X_i, muzzle velocity, muzzle retardation, and the exponent defining the shape of the drag curve.

$$Z_{R_i} = \frac{W_{Z_{(i-1,i)}}}{V_0(n-1)\left(\frac{dV}{ds}\right)_0}\left\{\frac{V_0 + \left(\frac{dV}{ds}\right)_0((n-1)R + X_i)}{\left(1 + n\left(\frac{dV}{ds}\right)_0 \frac{X_i}{V_0}\right)^{\frac{1}{n}}} - \frac{V_0 + \left(\frac{dV}{ds}\right)_0((n-1)R + X_{i-1})}{\left(1 + n\left(\frac{dV}{ds}\right)_0 \frac{X_{i-1}}{V_0}\right)^{\frac{1}{n}}}\right\} \, , n \neq 0, n \neq 1 \, . \tag{A-6}$$

$$Z_{R_i} = W_{Z_{(i-1,i)}}\left\{\frac{1}{\left(\frac{dV}{ds}\right)_0} \ln\left[\frac{V_0 + \left(\frac{dV}{ds}\right)_0 X_i}{V_0 + \left(\frac{dV}{ds}\right)_0 X_{i-1}}\right] + \left[\frac{R - X_i}{V_0 + \left(\frac{dV}{ds}\right)_0 X_i} - \frac{R - X_{i-1}}{V_0 + \left(\frac{dV}{ds}\right)_0 X_{i-1}}\right]\right\} , n = 1 \, . \tag{A-7}$$

$$Z_{R_i} = W_{Z_{(i-1,i)}}\left\{\left[\frac{-1}{\left(\frac{dV}{ds}\right)_0} + \frac{R - X_i}{V_0}\right] e^{-\left(\frac{dV}{ds}\right)_0 \frac{X_i}{V_0}} - \left[\frac{-1}{\left(\frac{dV}{ds}\right)_0} + \frac{R - X_{i-1}}{V_0}\right] e^{-\left(\frac{dV}{ds}\right)_0 \frac{X_{i-1}}{V_0}}\right\} , n = 0 \, . \tag{A-8}$$

[1] Weinacht PA. Direct-fire trajectory model for supersonic, transonic, and subsonic projectile flight. Aberdeen Proving Ground (MD): Army Research Laboratory (US); 2014 July. Report No.: ARL-TR-6998.

Appendix B. Supplementary Monte Carlo Results

Figures B-1 through B-4 show the standard deviation of the Equivalent Constant Crosswind (σ_{ECC}) versus range and examining the changes to σ_{ECC} with changes in drag coefficient exponent, muzzle velocity, projectile mass, and subsonic drag coefficient. The drag coefficient exponents and masses were chosen from among a list of fielded small-arms projectiles and thus are not evenly spaced.

Changing the drag coefficient exponent alone has very little effect on σ_{ECC} (approximately 1%) at any range, as shown in Fig. B-1.

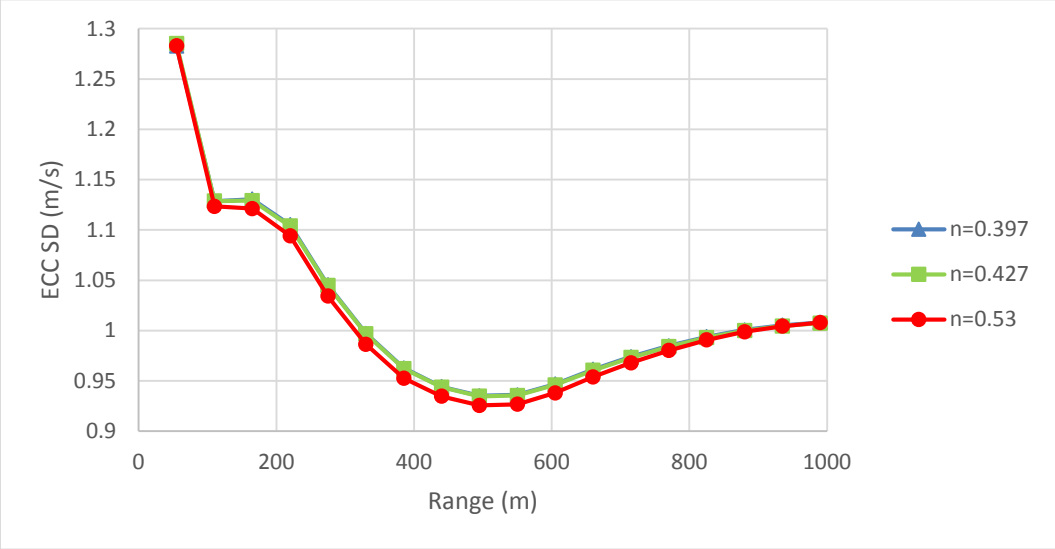

Fig. B-1 Comparison of different values of n

Changing the projectile's muzzle velocity has more of an effect on the value of σ_{ECC} than changing the drag coefficient exponent (up to 5% in the most extreme cases examined), but that effect is seen mostly at extended ranges (Fig. B-2). Even at the largest, though, the effects on σ_{ECC} induced by increasing or decreasing muzzle velocity are dwarfed by the effects of changing wind standard deviation and spatial correlation.

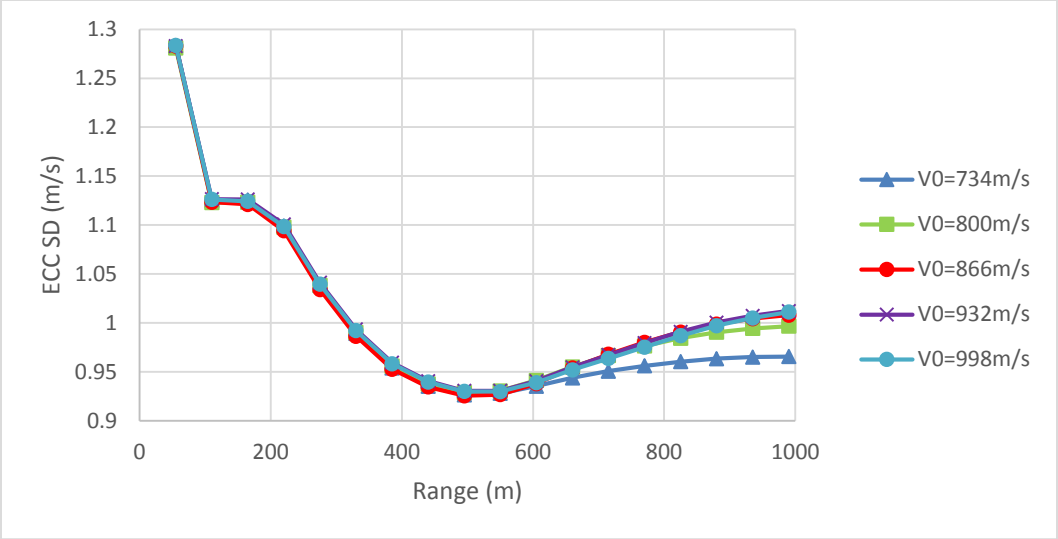

Fig. B-2 Comparison of different values of V_0

Changing projectile mass has very little effect on σ_{ECC} (at most between 1% and 2%) (Fig. B-3). The observed differences in σ_{ECC} come from the effect of changing mass on lag time, which is a primary driver of deflection due to crosswind.

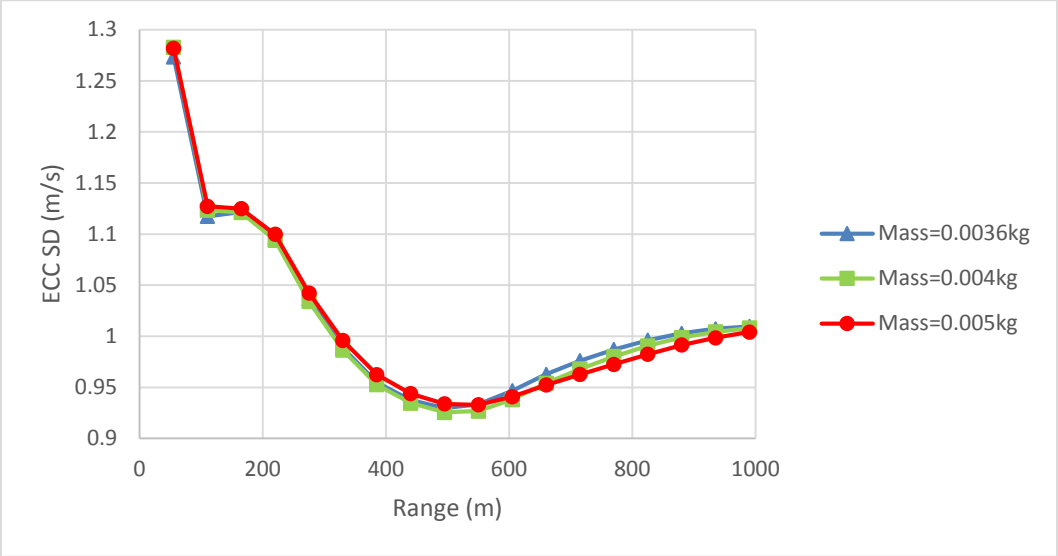

Fig. B-3 Comparison of different projectile masses

The subsonic drag coefficient plays no role in the trajectory until the range at which the projectile passes into the transonic drag regime, so Fig. B-4 shows a perfect overlap of all 3 cases until almost 600 m. The difference in σ_{ECC} observed thereafter between different cases does not exceed 0.5%.

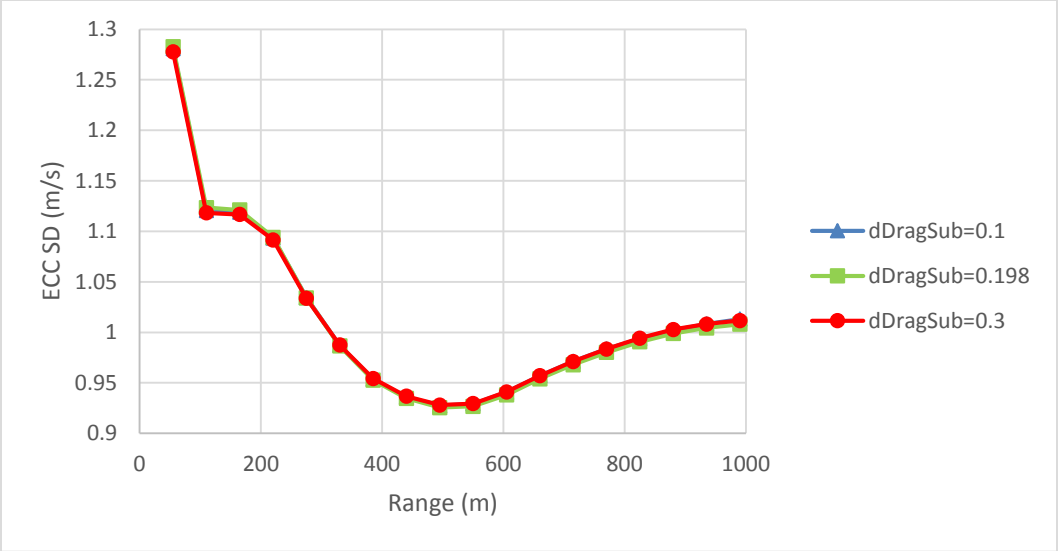

Fig. B-4 Comparison of different subsonic drag coefficients

Appendix C. Independent and Autoregressive Models

C.1 Independent Measurements

The simplest choice was to draw the wind at each station independently using μ_n and σ_n. This guaranteed that the behavior of the wind at each station was as observed.

To assess how well this independent model performed, we calculated the Equivalent Constant Crosswind (ECC) values across the range in question for each variable wind profile generated (ECC_I), aggregated them, and computed their mean and standard deviation to compare with those of the observed data. Figure C-1 shows μ_{ECC_B} and μ_{ECC_I} versus range, and Fig. C-2 shows σ_{ECC_B} and σ_{ECC_I} versus range.

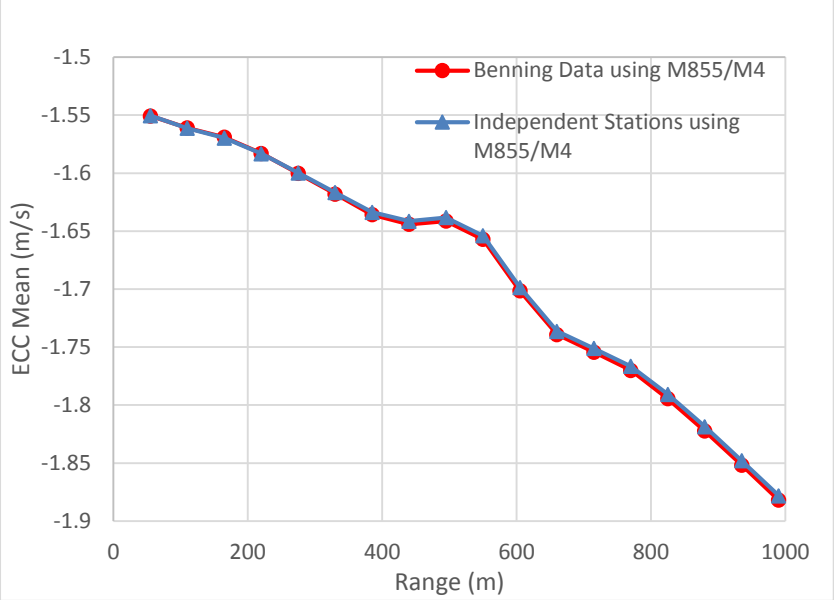

Fig. C-1 Comparison of μ_{ECC_B} and μ_{ECC_I}

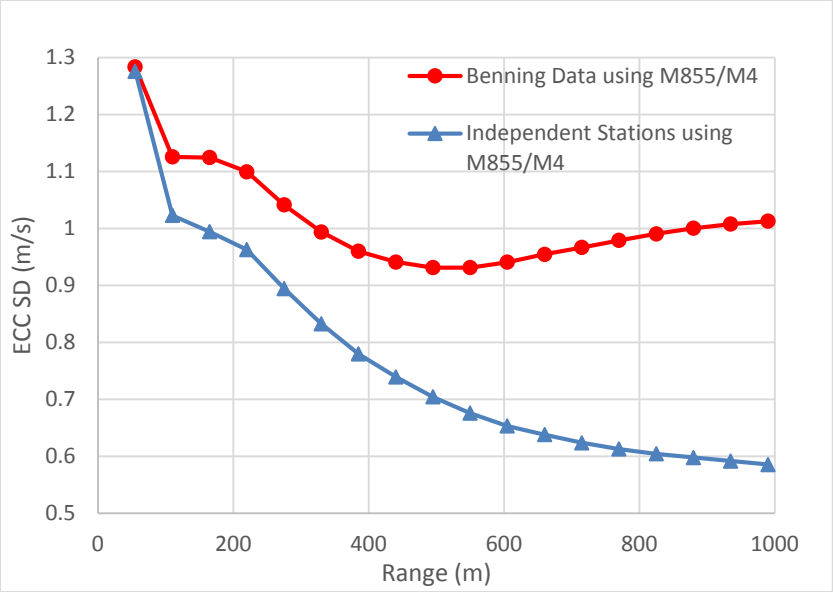

Fig. C-2 Comparison of σ_{ECC_B} and σ_{ECC_I}

μ_{ECC_B} and μ_{ECC_I} were within 0.3% of each other at all ranges, but σ_{ECC_B} and σ_{ECC_I} diverged with range, reaching a discrepancy of more than 40% by the maximum range. There is much more variation in ECC_B than in ECC_I. This is at least in part due to ECC_I not taking into account the correlation values between stations that we calculated in Section 2 of the main report. Including those correlations called for a more sophisticated model.

C.2 First-Order Autoregressive Model

An autoregressive model takes into account the correlation between measurements. The basic form of a first-order autoregressive model (so-called because it takes into account the first previous value to generate the next value) generates a sequence of values, X_n, each with zero mean and unit variance, which depend upon the previous states of the sequence, a set of correlation coefficients ($\rho_{n,m}$), and a normally distributed white-noise process with zero mean and unit variance (G_n).[1]

$$X_n = \rho_{n-1,n} X_{n-1} + G_n \sqrt{1 - \rho_{n-1,n}{}^2}\,. \qquad \text{(C-1)}$$

X_1 is simply drawn against a normal distribution with zero mean and unit variance. If we want the members of the sequence X_n to have a different mean and standard deviation (denoted μ_X and σ_X, respectively), we simply transform the sequence in the following way:

[1]Deserno M. How to generate exponentially correlated Gaussian random numbers. Los Angeles (CA): UCLA Department of Chemistry and Biochemistry; 2002 Aug [accessed 2016 Jan 28]. http//www.cmu .edu/biolphys/deserno/pdf/corr _gaussian_random.pdf.

$$W_n = \mu_X + \sigma_X X_n \,. \qquad \text{(C-2)}$$

In our case, the members of the sequence represent the anemometers in ascending order. Since each member of the sequence W_n has the same mean and standard deviation and our anemometer measurements have different means and standard deviations, we need a modified formula to preserve those measurements.[1]

$$W_n = \rho_{n-1,n}\frac{\sigma_n}{\sigma_{n-1}}(W_{n-1} - \mu_{n-1}) + \sigma_n G_n\sqrt{1-\rho_{n-1,n}{}^2} + \mu_n \,. \qquad \text{(C-3)}$$

Deserno[1] did not include the calculations, but we can easily show that in this formulation, each member of the sequence, W_n, has mean μ_n and standard deviation σ_n (variance $\sigma_n{}^2$). First in the sequence is the mean.

$$E(W_n) = E(\rho_{n-1,n}\frac{\sigma_n}{\sigma_{n-1}}(W_{n-1} - \mu_{n-1}) + \sigma_n G_n\sqrt{1-\rho_{n-1,n}{}^2} + \mu_n) \,.$$

$$E(W_n) = E(\rho_{n-1,n}\frac{\sigma_n}{\sigma_{n-1}}(W_{n-1} - \mu_{n-1})) + E(\sigma_n G_n\sqrt{1-\rho_{n-1,n}{}^2}) + E(\mu_n) \,.$$

$$E(W_n) = \rho_{n-1,n}\frac{\sigma_n}{\sigma_{n-1}}E(W_{n-1} - \mu_{n-1}) + \sigma_n\sqrt{1-\rho_{n-1,n}{}^2}E(G_n) + \mu_n \,.$$

$$E(W_n) = \rho_{n-1,n}\frac{\sigma_n}{\sigma_{n-1}}(E(W_{n-1}) - E(\mu_{n-1})) + \sigma_n\sqrt{1-\rho_{n-1,n}{}^2}\cdot 0 + \mu_n \,.$$

$$E(W_n) = \rho_{n-1,n}\frac{\sigma_n}{\sigma_{n-1}}(\mu_{n-1} - \mu_{n-1}) + \mu_n \,.$$

$$E(W_n) = \mu_n \,.$$

Next is the variance (using the fact that G_n and W_n are independent, and therefore have zero covariance).

$$Var(W_n) = E[(\rho_{n-1,n}\frac{\sigma_n}{\sigma_{n-1}}(W_{n-1} - \mu_{n-1}) + \sigma_n G_n\sqrt{1-\rho_{n-1,n}{}^2} + \mu_n - \mu_n)^2] \,.$$

$$Var(W_n) = E[(\rho_{n-1,n}{}^2\frac{\sigma_n{}^2}{\sigma_{n-1}{}^2}(W_{n-1} - \mu_{n-1})^2 + \sigma_n{}^2 G_n{}^2(1-\rho_{n-1,n}{}^2) + 2\rho_{n-1,n}\frac{\sigma_n{}^2}{\sigma_{n-1}}\sqrt{1-\rho_{n-1,n}{}^2}(W_{n-1} - \mu_{n-1})G_n]$$

$$Var(W_n) = \rho_{n-1,n}{}^2\frac{\sigma_n{}^2}{\sigma_{n-1}{}^2}E(W_{n-1} - \mu_{n-1})^2 + \sigma_n{}^2(1-\rho_{n-1,n}{}^2)E(G_n{}^2) + 2\rho_{n-1,n}\frac{\sigma_n{}^2}{\sigma_{n-1}}\sqrt{1-\rho_{n-1,n}{}^2}E((W_{n-1} - \mu_{n-1})G_n)$$

$$Var(W_n) = \rho_{n-1,n}{}^2\sigma_n{}^2 + \sigma_n{}^2(1-\rho_{n-1,n}{}^2) + 2\rho_{n-1,n}\frac{\sigma_n{}^2}{\sigma_{n-1}}\sqrt{1-\rho_{n-1,n}{}^2}\cdot 0 \,.$$

$$Var(W_n) = \rho_{n-1,n}{}^2\sigma_n{}^2 + \sigma_n{}^2(1-\rho_{n-1,n}{}^2) \,.$$

$$Var(W_n) = \sigma_n{}^2 \,.$$

Using μ_n, σ_n, and $\rho_{n,m}$ from Section 2 of the report, we can now implement the first-order autoregressive model and compare its ECC results (ECC_{AR1}) with the observed data (for all subsequent models we will only show the charts illustrating σ_{ECC} because μ_{ECC} was accurate to within 0.5% at any range using any proposed model). This is shown in Fig. C-3 along with the results from the independent model.

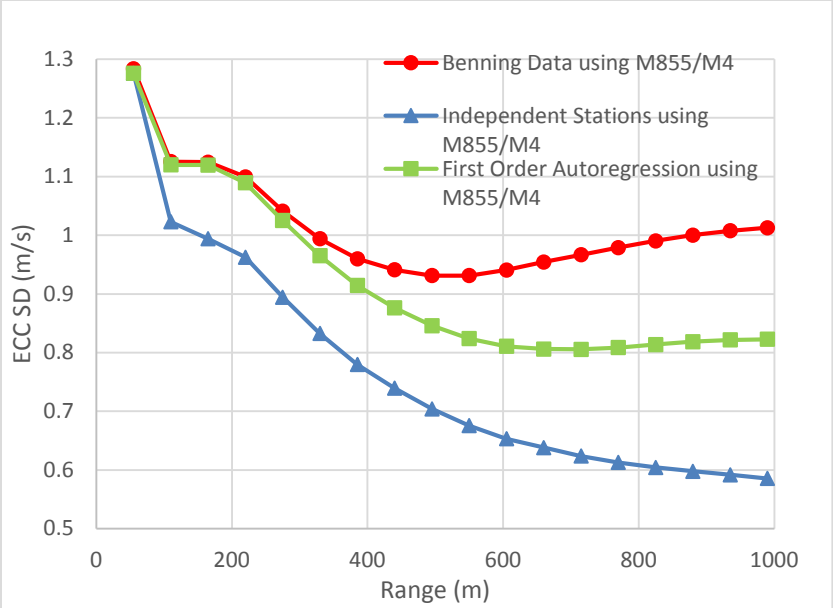

Fig. C-3 Comparison of σ_{ECC_B}, σ_{ECC_I}, and $\sigma_{ECC_{AR1}}$

As shown, $\sigma_{ECC_{AR1}}$ diverges far less from σ_{ECC_B} across all ranges than σ_{ECC_I} but it still underestimates σ_{ECC_B} by almost 20% at the longer ranges. This raises the question of whether it is valuable to take more correlations into account.

C.3 Higher-Order Autoregressive Models

Deserno[1] only provides the technique to implement a first-order autoregressive model. We derived a general formula to model a given order of autoregression and also preserve μ_n and σ_n. As an example, we look at extending from a first-order to a second-order autoregressive model. That would involve an expression like the following[2]:

$$W_n = \rho_{n-1,n}\frac{\sigma_n}{\sigma_{n-1}}(W_{n-1}-\mu_{n-1}) + \sigma_n G_{n,1}\sqrt{1-\rho_{n-1,n}{}^2} + \rho_{n-2,n}\frac{\sigma_n}{\sigma_{n-2}}(W_{n-2}-\mu_{n-2}) + \sigma_n G_{n,2}\sqrt{1-\rho_{n-2,n}{}^2} + \mu_n . \quad \text{(C-4)}$$

But that expression, though it takes into account the previous 2 values of W_n and the corresponding correlation coefficients and preserves μ_n (this can be verified analogously to the process shown in Section 5.2 and is not shown here), does not preserve the variance as σ_n.[2] Finding the variance of Eq. C-4 begins as it did in the first-order case, and the steps relying on independence of the G_n terms with the other variables will be omitted.

$$Var(W_n) = E(\rho_{n-1,n}\frac{\sigma_n}{\sigma_{n-1}}(W_{n-1}-\mu_{n-1}) + \sigma_n G_{n,1}\sqrt{1-\rho_{n-1,n}{}^2} + \rho_{n-2,n}\frac{\sigma_n}{\sigma_{n-2}}(W_{n-2}-\mu_{n-2}) + \sigma_n G_{n,2}\sqrt{1-\rho_{n-2,n}{}^2})^2 \ .$$

[2] We specify $G_{n,1}$ and $G_{n,2}$ to clarify that the white noise processes are separate and independent.

$$Var(W_n) = E(\rho_{n-1,n}{}^2 \frac{\sigma_n{}^2}{\sigma_{n-1}{}^2}(W_{n-1} - \mu_{n-1})^2 + \sigma_n{}^2 G_{n,1}{}^2(1 - \rho_{n-1,n}{}^2) + \rho_{n-2,n}{}^2 \frac{\sigma_n{}^2}{\sigma_{n-2}{}^2}(W_{n-2} - \mu_{n-2})^2$$
$$+\sigma_n{}^2 G_{n,2}{}^2(1 - \rho_{n-2,n}{}^2) + 2 \cdot \rho_{n-1,n}\rho_{n-2,n}\frac{\sigma_n{}^2}{\sigma_{n-1}\sigma_{n-2}}(W_{n-1} - \mu_{n-1})(W_{n-2} - \mu_{n-2})) .$$

$$Var(W_n) = 2\sigma_n{}^2 + 2 \cdot \rho_{n-1,n}\rho_{n-2,n}\frac{\sigma_n{}^2}{\sigma_{n-1}\sigma_{n-2}} E((W_{n-1} - \mu_{n-1})(W_{n-2} - \mu_{n-2})).$$

$$Var(W_n) = 2\sigma_n{}^2 + 2 \cdot \rho_{n-1,n}\rho_{n-2,n}\frac{\sigma_n{}^2}{\sigma_{n-1}\sigma_{n-2}}\rho_{n-2,n-1}\sigma_{n-1}\sigma_{n-2} .$$

$$Var(W_n) = 2\sigma_n{}^2 + 2 \cdot \rho_{n-1,n}\rho_{n-2,n}\rho_{n-2,n-1}\sigma_n{}^2 .$$

$$Var(W_n) = \sigma_n{}^2(2 + 2\rho_{n-1,n}\rho_{n-2,n}\rho_{n-2,n-1}) .$$

This points the way forward for how to modify our expression to preserve the observed means and standard deviations at the stations, which is accomplished in the following expression:

$$W_n = \frac{\rho_{n-1,n}\frac{\sigma_n}{\sigma_{n-1}}(W_{n-1} - \mu_{n-1}) + \sigma_n G_{n,1}\sqrt{1-\rho_{n-1,n}{}^2} + \rho_{n-2,n}\frac{\sigma_n}{\sigma_{n-2}}(W_{n-2} - \mu_{n-2}) + \sigma_n G_{n,2}\sqrt{1-\rho_{n-2,n}{}^2}}{\sqrt{2 + 2\rho_{n-1,n}\rho_{n-2,n}\rho_{n-2,n-1}}} + \mu_n . \quad \text{(C-5)}$$

More generally, we can derive an expression that will preserve μ_n and σ_n for any order p of autoregression. We assume that for an autoregressive model of order p, if $n \leq p + 1$, the model will use all available previous measurements to generate the n^{th} measurement.

$$W_n = \mu_n + \sum_{i=1}^{\mathrm{L}} \frac{(\rho_{n-i,n}\frac{\sigma_n}{\sigma_{n-i}}(W_{n-i} - \mu_{n-i}) + \sigma_n G_{n,i}\sqrt{1-\rho_{n-i,n}{}^2})}{C} , \quad \text{(C-6)}$$

where L and C are constants determined by

$$L = \min(p, n-1) . \quad \text{(C-7)}$$

$$C = \sqrt{\mathrm{L} + \sum_{i=1}^{\mathrm{L}-1}\sum_{j=i+1}^{\mathrm{L}} 2\rho_{n-i,n}\rho_{n-j,n}\rho_{n-j,n-i}} . \quad \text{(C-8)}$$

With this expression in hand, we can implement higher-order autoregressive models and compare their ECC results with the observed data. Fig. C-4 shows the results from using autoregressive models up to order 5. All curves represent ECC determined using the M855/M4 ammunition/weapon configuration.

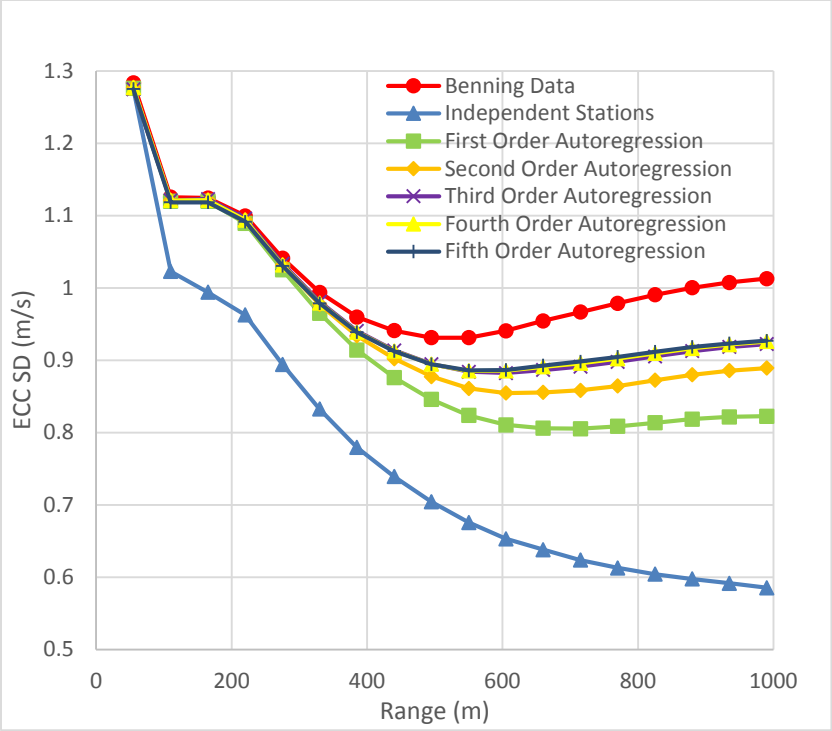

Fig. C-4 Multiple-order autoregression σ_{ECC} results

Each higher order of autoregression produces results that are marginally closer to the observed data than the next lower level, but there is little difference between the models' performance past the third-order model. The fourth- and fifth-order models overlap almost completely and produce only minimal gains over the third-order model. $\sigma_{ECC_{AR3}}$ stays within 10% of σ_{ECC_B} across the whole range, though it persistently underestimates σ_{ECC_B} (as do all of the models' results).

Figure C-4 and the persistent gap between the models' results and the observed results raise the question of whether the models tend to accumulate errors with increasing range or whether some other phenomenon could account for the gap. One way we can address that question is to reverse the order of the anemometers and determine σ_{ECC_B} if we assumed that we were standing at station A_{10} and looking at station A_{10}. Fig. C-5 shows these results, which once again assume the M855/M4 configuration.

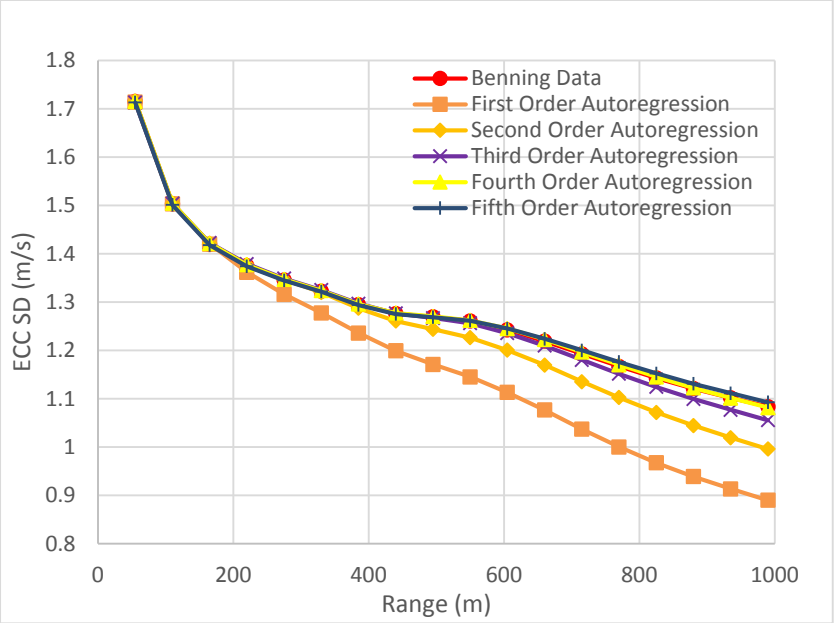

Fig. C-5 Reversed direction multiple-order autoregression σ_{ECC} results

$\sigma_{ECC_{AR4}}$ stays consistently within 0.4% of σ_{ECC_B} across all ranges when the anemometers are reversed.

The model's close adherence to the observed data in this case should not be overemphasized, however. There still remains a gap between the modeled results and the observed results in some cases, and upon examination, while they often do a good job of replicating the behavior of the wind data from Fort Benning, the autoregressive models of all orders have drawbacks that significantly limit the reliability of their performance in general.

Because the autoregressive models implicitly order the wind measurements and only incorporate crosswinds from one direction when generating new measurements, they are not equipped to model changes in correlation that are otherwise unpredictable from the foregoing data. In Table 2 of the main report, the average correlation between adjacent stations from A_1 to A_5 is 0.25 while the average correlation between adjacent stations from A_6 to A_{10} is 0.48. Nothing about the correlations between A_1 and A_5 indicates such a jump in correlation for the subsequent stations, and, looking in the other direction, nothing about the correlations between A_6 and A_{10} indicates such a drop in correlation for subsequent stations. Since the correlations are not inherently directional, they cannot be a function of the preceding correlations (for whichever ordering is arbitrarily chosen) and cannot be preserved without a model that takes them all into account from the start.

1 (PDF) DEFENSE TECHNICAL INFORMATION CTR DTIC OCA

2 (PDF) DIRECTOR US ARMY RESEARCH LAB RDRL CIO LL IMAL HRA MAIL & RECORDS MGMT

1 (PDF) GOVT PRINTG OFC A MALHOTRA

7 (PDF) DIR USARL RDRL CIH C R YAGER RDRL WML A T FARGUS WF OBERLE M ARTHUR L STROHM B BREECH RDRL WML H J NEWILL

INTENTIONALLY LEFT BLANK.